6-17-2013

Ontogenetic Scaling of the Olfactory Antennae and Flicking Behavior of the Shore Crab, *Hemigrapsus oregonensis*

Lindsay D. Waldrop
Chapman University, waldrop@chapman.edu

Recommended Citation

L.D. Waldrop. 2013. Ontogenetic scaling of the olfactory antennae and flicking behavior of the shore crab, *Hemigrapsus oregonensis. Chemical Senses* 38(6): 541-550. https://doi.org/10.1093/chemse/bjt024

Ontogenetic Scaling of the Olfactory Antennae and Flicking Behavior of the Shore Crab, *Hemigrapsus oregonensis*

Ontogenetic scaling of the olfactory antennae and flicking behavior of the shore crab, *Hemigrapsus oregonensis*

Lindsay D. Waldrop[1]

[1]**Department of Integrative Biology, Univ. of California, Berkeley. Correspondence to be sent to: Dept. of Mathematics, CB#3250, Univ. of North Carolina at Chapel Hill. Email: lwaldrop[at]email.unc.edu**

ABSTRACT

Malacostracan crustaceans such as crabs flick antennae with arrays of olfactory sensilla called aesthetascs through the water to sense odors. Flicking by crabs consists of a quick downstroke, in which aesthetascs are deflected laterally (splayed), and a slower, reversed return stroke, in which aesthetascs clump together. This motion causes water to be flushed within then held in between aesthetascs to deliver odor molecules to olfactory receptors. Although this odor sampling method relies on a narrow range of speeds, sizes, and specific arrangements of aesthetascs, most crabs dramatically change these during ontogeny. In this study, the morphometrics of the aesthetascs, array, and antennae and the flicking kinematics of the Oregon shore crab, *Hemigrapsus oregonensis* (Decapoda: Brachyura), are examined to determine their scaling relationships during ontogeny. The morphometrics of the array and antennae increase more slowly than would be predicted by isometry. Juvenile crabs' aesthetascs splay relatively further apart than adults, likely due to changing material properties of aesthetasc cuticle during growth. These results suggest that disproportionate growth and altered aesthetasc splay during flicking will mediate the size changes due to growth that would otherwise lead to a loss of function.

Keywords: antennule, biofluid dynamics, decapoda, olfaction, ontogeny, sniffing

Preprint version of published paper in *Chemical Senses* 38: 541-550, 2013.

INTRODUCTION

Many crustaceans use dissolved chemical cues (odors) as a source of information throughout their ontogeny (Schmidt and Ache, 1979; Dusenbery, 1992; Atema, 1995; Zimmer and Butman, 2000). Larvae use olfactory cues to select a suitable habitat for settlement from the water column, to avoid predation, and to find food (Diaz et al., 1999; Pardieck et al., 1999; Ferner et al., 2005; Lecchini et al., 2010). Adult crustaceans also rely on odors to locate food, to interact with conspecifics, and to mediate reproductive behaviors (Hazlett, 1969; Caldwell, 1979; Gleeson, 1980; Gherardi et al., 2005; Atema and Steinbach, 2007; Gherardi and Tricarico, 2007; Shabani et al., 2009; Skog, 2009).

A key aspect of olfaction is the process by which odor molecules are acquired by an organism. In order to use the information contained in odors, odor molecules must be captured from the surrounding environment (Moore et al., 1991; Koehl, 2006). The act of odor capture is mediated by physical processes and, for many animals, is accomplished with a specialized chemosensory organ that intermittently samples the surrounding fluid.

Broadly, intermittent odor sampling, or 'sniffing' is characterized by rapid fluid flow induced by an animal that provides a way to carry odor molecules to olfactory surfaces (Schmidt and Ache, 1979). Intermittent sampling physically controls the flow of information from the environment to the olfactory system by introducing temporal structure to the delivery of odor molecules to sensory structures (Kepecs et al., 2006; Wachowiak, 2011). Beyond simply delivering odor molecules to olfactory surfaces, there is evidence that sniffing plays a role in how olfactory information is encoded by olfactory neurons and ultimately perceived by animals, specifically to deal with confounding variables such as respiration and possibly environmental fluid flows (Schoenfeld, 2006; Wachowiak, 2011). Sniffing also creates unique

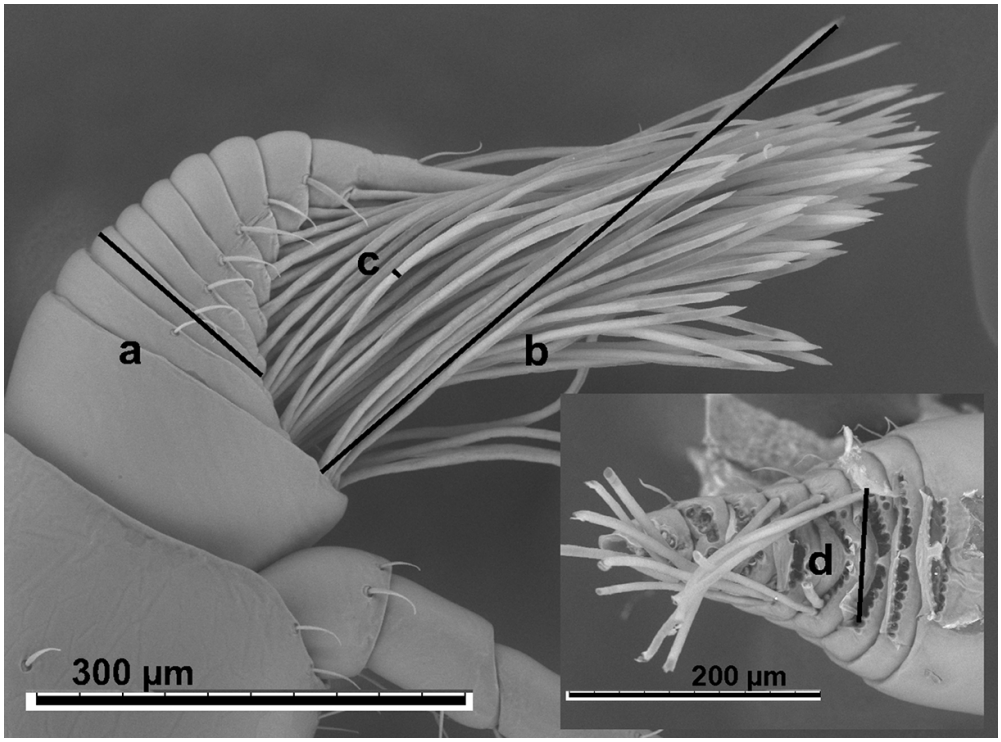

Figure 1. Scanning electron micrograph of side view of *Hemigrapsus oregonensis* antennule (inset: front view with aesthetascs removed) with morphometric measurements indicated by letter: (a) antennule side (thickness); (b) aesthetasc length; (c) aesthetasc diameter; (d) array width.

spatiotemporal patterns of odors based on the distribution of odor molecules in a turbulent plume, which likely aids in orienting towards and tracking odor sources (Moore et al., 1991; Koehl, 2006; Keller et al., 2003).

Crustacean antennule design

Malacostracan crustaceans sniff by moving a specialized chemosensory organ (first antenna or antennule, Fig. 1), studded with an array of long, flexible chemosensory sensilla (aesthetascs), through the water in a motion called 'flicking' (Snow, 1973; Schmidt and Ache, 1979; Derby and Atema, 1988). Aesthetascs are innervated with dendrites from chemosensory neurons; dendrites are separated by a thin layer of cuticle from the outside environment (Hallberg et al., 1997; Hallberg and Skog, 2011). This layer of cuticle is permeable to several types of odorants and ions (Gleeson, 1982; Gleeson et al., 2000a,b). Aesthetascs are arranged in rows with regular spacings between both aesthetascs and rows of aesthetascs on one branch of the biramus antennule.

For marine decapods, antennule flicking involves a rapid downstroke (Fig. 2A) and slower return stroke (Fig. 2B) in the opposite direction (Snow, 1973; Koehl, 2006). Like antennule morphology, the kinematics of flicking also vary between crustacean species. In crabs, the downstroke is about twice the speed of the return stroke. During the downstroke, the aesthetasc array is directly upstream and hydrodynamic drag causes the flexible aesthetascs to deflect laterally, increasing the distances between individual aesthetascs. The direction of the return stroke is reversed, causing the aesthetascs to be tightly clumped together (Snow, 1973).

Fluid dynamics of sniffing

Odor molecules near the antennules are transported to the surfaces of the aesthetascs during flicking by a combination of molecular diffusion and water currents that are regulated by the interactions of water with the solid features of the array (Atema, 1995; Goldman and Patek, 2002; Koehl, 2006). During antennule movement, a thin layer of water adheres to the solid surfaces of the aesthetascs ('no-slip' condition) and is sheared, creating a gradient of water velocities around each aesthetasc (boundary layer). The thickness

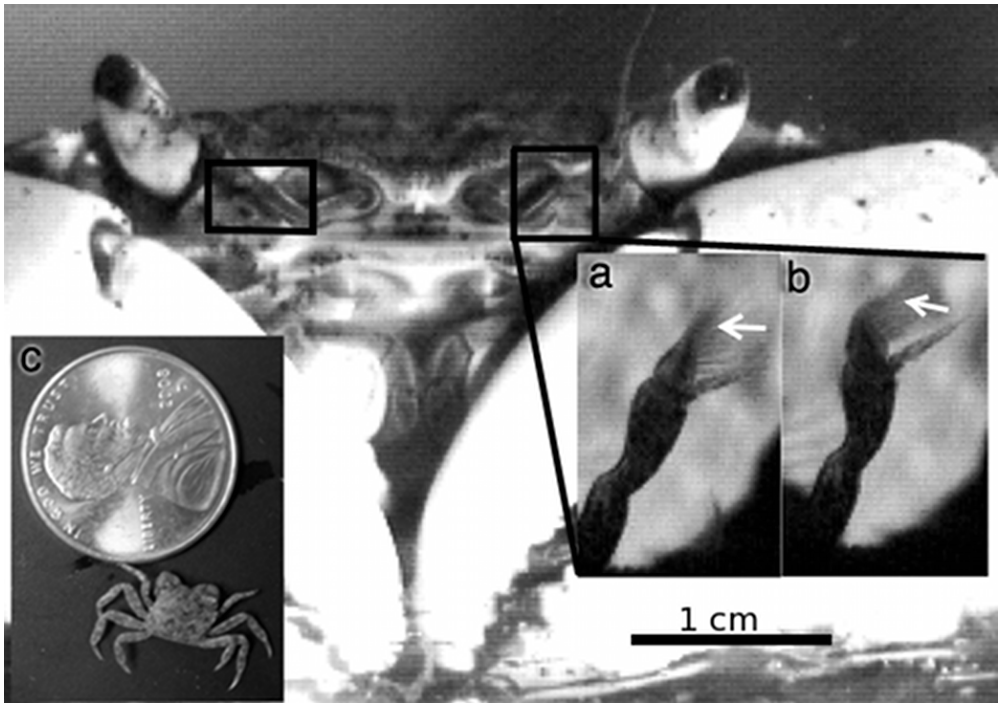

Figure 2. Anterior view of adult *Hemigrapsus oregonensis*. Antennules are enclosed by black boxes. (a) Close-up view of antennule during downstroke of flick showing aesthetascs (marked by white arrow) spread apart; (b) close-up view of antennule during return stroke of flick, showing aesthetascs (marked by white arrow) clumped together; (c) juvenile *H. oregonensis* individual with penny for scale.

of each boundary layer can be described as a function of the Reynolds number (*Re*):

$$Re = \frac{Ud\rho}{\mu} \tag{1}$$

where U is the velocity relative to the aesthetascs, and d is the aesthetasc diameter, and μ and ρ are the dynamic viscosity and density of the fluid, respectively (Vogel, 1994). Relative boundary layer thickness is proportional to $Re^{-1/2}$; faster velocities result in thinner boundary layers and thicker boundary layers for slower velocities.

The fast movement ($Re \approx 1$) of the antennule during the downstroke creates thinner boundary layers between aesthetascs, allowing new water to flow in between the aesthetascs and displace water from previous flicks. Because aesthetascs are closer to their neighbors during the slower return stroke ($Re \approx 0.1$), the relatively thicker boundary layers around the aesthetascs interact, diverting water around the array and trapping a sample of water within the array (Koehl, 2006).

Each flick represents a discrete, intermittent sampling cycle or sniff as fluid is captured during the downstroke then held against the chemosensory surfaces during the return stroke, akin to sniffing in other animals (Koehl, 2006). This function reduces the boundary layers around each aesthetasc to allow more of the sensory surface to be exposed to new odor-containing fluid (Atema, 1995; Koehl, 2006). During the time fluid is trapped in the array, odor molecules diffuse to the surfaces of each aesthetasc and enhancing the number of molecules captured per cycle (Stacey et al., 2002; Schuech et al., 2012).

Previous research on fluid flow within hair arrays shows that *Re* and other aspects of array design affect the amount of fluid that flows within an array (Cheer and Koehl, 1987a; Loudon et al., 1994). Cheer and Koehl (1987a,b) developed models to describe fluid flow within a finite array of cylinders by measuring the fluid flowing through the array divided by possible flow in the absence of an array (leakiness). When *Re* increased between 0.01 and 1, the leakiness of an array increased disproportionately compared to increases flow outside this *Re* range (Cheer and Koehl, 1987a,b; Loudon et al., 1994). Small changes in the ratio of gap width between hairs to diameter of the hairs also had profound effects on array leakiness; larger ratios, or hairs spaced further apart, produced much leakier array than smaller ratios

(Cheer and Koehl, 1987a,b). For many decapods, *Re*'s of antennule flicking fall within the range where small changes in speed and gap width are especially effective at changing fluid flow within the array. Deflection, or splay, of aesthetascs seen during the downstroke of brachyuran and anomuran crabs could also serve to increase flow within the array during the downstroke (Koehl, 2006). Decreases in speed and gap width during the return stroke also decrease fluid flow within the array.

Scaling and the function of antennules

Many animals, including crustaceans, undergo a change in size during their lifetimes through growth. The Oregon shore crab, *Hemigrapsus oregonensis* (Dana 1852), grows from a two-millimeter post-settlement juvenile to a 35-millimeter adult (Fig. 2C). *H. oregonensis* juveniles share similar predation threats, conspecific interactions, and habitat preference as adults, suggesting that they have similar sensory ecologies (Hart, 1935). The antennules of juveniles are absolutely much smaller than those of adult animals.

Having a much smaller body size, and by extension smaller antennule features, will result in lower Re during antennule flicking by decreasing the characteristic length d in equation 1. If juveniles' antennules were isometrically scaled compared to adults, crabs would begin life with antennules not capable of producing *Re* high enough to force fluid within the array during the downstroke ($Re < 0.1$), limiting the amount of their sensory surfaces able to access new odor samples. The aesthetasc arrays of juveniles would also have a smaller gap-width-to-diameter ratio, further exacerbating the effects of their small size on fluid flow through the array.

Allometric scaling of antennule features such as aesthetasc diameter and length could lessen the absolute change that these features experience during growth. If these features grow more slowly than expected by isometry, juvenile animals would have both larger antennules relative to their body size and larger in an absolute scale, possibly allowing the *Re* of the downstroke to remain in the range functionally important for sniffing (Mead and Koehl, 2000).

Likewise, altered gap widths between aesthetascs during flicking could compensate for smaller aesthetasc features and still allow water to penetrate the array. How far aesthetascs splay depends on several variables: the relative proportions of aesthetasc structural features and material properties of aesthetasc cuticle. The distance an individual aesthetasc is deflected at its free end, D, can be modeled as a bending beam under a hydrodynamic drag force, F, distributed along the aesthetasc's length is:

$$D = \frac{FL^3}{8EI} \tag{2}$$

where L is aesthetasc length, E is Young's modulus of aesthetasc chitin, and I is the second moment of area for a hollow tube (Wainwright et al., 1982; Vogel, 2003). Young's modulus is a measure of a material's stiffness, describing the relationship between stress and strain. I, which describes the distribution of material that would resist bending, for a hollow tube is:

$$I = \frac{\pi}{4}(R_i^4 - R_0^4) \tag{3}$$

where R_0 is the outer radius and R_i is the inner radius of the aesthetasc.

An important part of equation 2 is the flexural stiffness of the aesthetasc, EI, which represents both its structure through I, the second moment of area, and its material properties represented by Young's modulus, E. Either the material properties (changes in E) or the structure through allometric scaling (changes in I) could vary during ontogeny to produce altered splay ratios.

Since the ability to sniff, or intermittently sample odors, by crustaceans depends heavily on the morphology of the antennule and kinematics of flicking, predictions can be formed regarding the ability of juvenile crabs to discretely sample odors by examining changes in antennules during ontogeny. In this study, I investigate the changes in morphological and structural characteristics of antennules and kinematics of antennule flicking likely to impact sniffing during the ontogeny of the Oregon shore crab, *H. oregonensis*. It is likely that due to allometric growth of the antennules of juvenile crabs will continue to operate within the sensitive *Re* shared by other crustaceans despite a large change in body size during growth. Additionally, increasing the splay ratio of juvenile crabs would result in leakier arrays during the downstroke of flicking due to a change in either the structural or material properties of the aesthetascs.

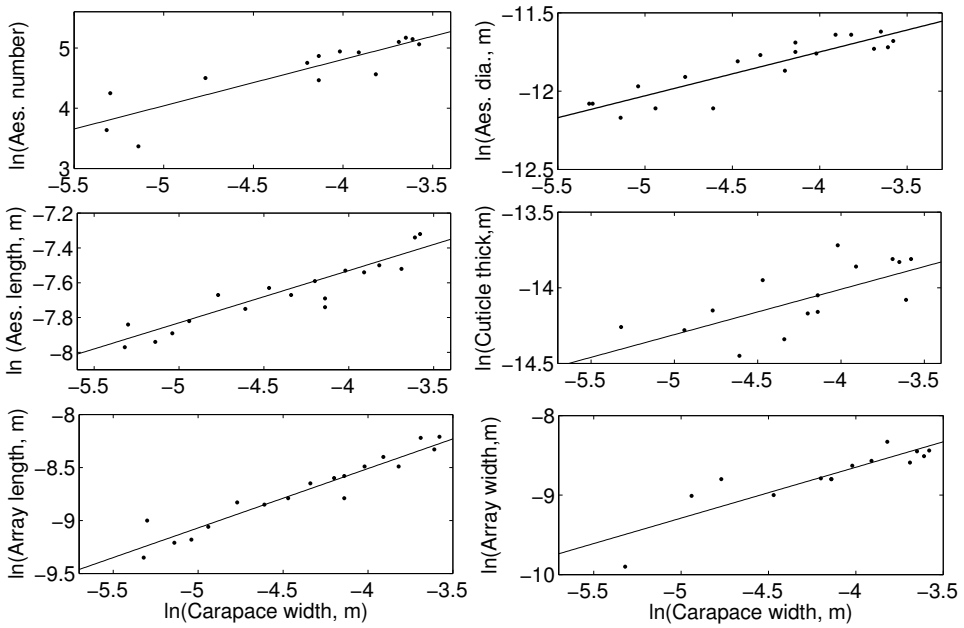

Figure 3. Select morphometric features measured vs. natural-log carapace width plots. Top left: Number of aesthetascs; top right: aesthetasc diameter; middle left: Aesthetasc length; middle right: aesthetasc cuticle thickness; bottom left: aesthetasc array length; bottom right: aesthetasc array width.

METHODS AND MATERIALS

Collection and maintenance of animals

Hemigrapsus oregonensis inter-molt individuals were collected from the shore during low tide on the Emeryville shoreline of the San Francisco Bay, CA, USA. Animals were grouped according to size and kept in containers of seawater with aeration at 12 °C. Animals were supplied with macro and micro algae and frozen shrimp.

The carapace width (used as an index of body size) of each animal was measured to the nearest 0.1 mm at the widest point (between the third distal carapace teeth) with standard digital calipers. Adult animals were sexed according to the shape of the abdomen, but small juvenile animals were not sexed due to insufficient differences in external anatomy. After kinematic observations were made, animals were relaxed in 14% $MgCl_2$ in isotonic seawater (Lincoln and Sheals, 1979). Both antennules were removed with forceps.

Scanning Electron Microscopy (SEM)

Antennules were taken from H. oregonensis individuals and photographed using scanning electron microscopy. Specimens of whole antennules from each crab were fixed for an hour in 2% glutaraldehyde in 0.1 M sodium cacodylate buffer, pH 7.2. Antennules were then post-fixed in 1% osmium tetroxide for one hour and washed with the sodium cacodylate buffer (Mead et al., 1999). The aesthetascs of one antennule from each crab were then removed with a scalpel, while the second antennule from each crab was left with intact aesthetascs. Specimens were then dehydrated in an alcohol series and dried in a Critical Point Dryer (Tousimis AutoSamdri 815). Micrographs of the aesthetasc-bearing segments of the antennules were taken using a Hitachi TM-1000 Environmental Scanning Electron Microscope with a 15 kV beam at various magnifications.

Morphometrics

Measurement of aesthetascs diameter, aesthetasc cuticle thickness, aesthetasc length, array width at the third segment were taken from SEMs (see Fig. 1 for measurements) using ImageJ (Abramoff et al., 2004) to the nearest 10^{-2} μm. Antennule size was measured as the length of the third aesthetasc-bearing segment distally from the base of the antennule in two linear dimensions: the antennule thickness and the array width. Each measurement represents either a single measurement where only one measurement

could be taken (antennule thickness, array width) or the average of three to five measurements on different aesthetascs of the same individual where multiple measurements could be taken (aesthetasc diameter, aesthetasc length, aesthetasc cuticle thickness).

The growth rate of each morphometric measurement was compared against the increase in carapace width (body size). The natural log of morphometric measurements for individual animal were plotted against the natural log of carapace width and regressions were calculated using the least-squares method of linear regression in the OpenOffice.org statistical package. The resulting slopes (uncertainty given as the standard error, s_e) were used to test for isometry where line slope would equal one. All measurements of length are expected to be proportional to carapace width and the null hypothesis of isometry is a slope (β_0) of one ($H_0 : \beta = \beta_0$). Slopes not equal to one indicate allometric growth ($H_a : \beta \neq \beta_0$).

To test the difference between the slopes of each regression against the expected slope, the standard method of testing the results of a linear regression against a presumed slope was used (Devore, 1987; Dodds et al., 2001). The t-value is calculated based on the assumption that two linearly-related variables exhibiting normal distributions would differ at least by as much as the expected and actual slopes (β_0 and β) vary:

$$t = \frac{\beta - \beta_0}{s_e} \tag{4}$$

P-values are then calculated from a student's bimodal t-distribution with $(n-2)$ degrees of freedom at $\alpha = 0.05$.

Kinematics

Antennule flicking by crabs were captured on video to analyze their movement. Crabs were starved for two to three days so they would be responsive to odors during filming. An individual crab's carapace widths were measured then the crab was placed in a small container of still seawater and allowed to acclimate for 15 minutes before filming. The container had a millimeter scale and was surrounded by a temperature bath. The size of the container limited animal movement but was large enough not to interfere with antennule movement. Animals smaller than eight mm in carapace width were glued to a small wooden dowel to limit movement and held in a small dish under a Wild Heerburgg dissecting microscope with a scale micrometer. The field was illuminated by fiber-optic light sources (Cole Parmer 9741-50) to minimize heating of the water bath. The temperature was monitored and held between $12-14\,^{\circ}$C during filming. Shrimp extract was prepared by placing several grams of frozen shrimp in 250 mL of water for half an hour and straining off the liquid. To illicit flicking behavior, a small amount of shrimp extract was dripped into the water. Flicking motions were captured with a RedLake MotionScope PCI 1000s camera (Redlake Inc., Tucson, AZ, USA) at 1000 frames per second.

Selected clips, those showing antennule flicking in the focal plane of the camera, were then digitized with Graphclick (Arizona Software, Inc.) and calibrated with a millimeter scale bar (large animals) or stage micrometer (small animals) located in each video clip. The antennule tip and based of aesthetasc array were digitized in each frame throughout the flicking event. Distances between positions from consecutive frames were divided by the time step between frames and compared to find the peak velocities, and the sum of distances measured in each frame was divided by the total time to find mean velocities.

Variable	n	**Slope** $\pm s_e$	r^2	y**-intercept**	p **(slope = 1)**	**95% confidence**
Antennule thickness	18	0.56 ± 0.04	0.91	-6.27 ± 0.19	< 0.0000001	0.44 - 0.68
Aesthetasc array ...						
Width	14	0.64 ± 0.1	0.78	-6.10 ± 0.41	< 0.0001	0.94 - 0.34
Length	12	0.54 ± 0.09	0.79	-5.92 ± 0.39	< 0.00002	0.27 - 0.81
Aesthetasc ...						
Diameter	19	0.28 ± 0.03	0.81	-10.6 ± 0.15	< 0.0000001	0.18 - 0.38
Length	18	0.30 ± 0.03	0.86	-6.36 ± 0.13	< 0.0000001	0.20 - 0.40
Cuticle thickness	15	0.30 ± 0.09	0.48	-12.8 ± 0.37	< 0.00001	0.04-0.56
Hair number	14	0.77 ± 0.12	0.78	7.89 ± 0.27	0.2	0.67 - 0.87

Table 1. Summary of sample size (n), regression slopes ($\pm$ standard error, s_e), correlation coefficients (r^2), y-intercepts, 95% confidence intervals for slope and significance for seven measured features.

Out of several video clips, three to five flicking events were digitized per animal and an average mean and peak velocities were calculated for each of the downstroke and return stroke movements for every animal.

To estimate the distance between the aesthetascs of the array during flicking, two splay ratios were calculated per animal. The edges of the aesthetasc array were selected in Graphclick by taking single frames of the antennule where the splay was greatest during the downstroke. The distances between the tips and bases of the aesthetascs were calculated from digitized positions. The distances of tips of the aesthetascs were divided by the length of the array base to find the splay ratio. Two splay ratios were calculated from two orientations: the side view (antennule flicking parallel to the focal plane), and front view (antennule flicking normal to the focal plane). Values represent the average of two to five measurements per individual crab. The downstroke and return velocities were used to calculate Reynolds numbers using a kinematic viscosity of seawater (1.20×10^{-6} m^2 s^{-1}) at 30‰ and 15 °C (Vogel, 1994).

RESULTS

Antennule morphology

Figure 3 plots select features, and Table 1 summarizes measurements of morphological features and reports results of natural log plots (slopes, *y*-intercepts, correlation coefficients, and confidence intervals). All features measured in Table 1 had slopes that differed significantly from the slope expected for isometry ($m = 1$). For the size range in this study (3.9 to 27 mm), the antennules of the smallest juveniles are 87 μm wide and increase to 240 μm by adulthood. Aesthetasc lengths vary during growth from 347 to 648 μm, and aesthetasc diameters vary from 5.69 to 8.1 μm. During growth, antennules also add aesthetasc-bearing segments to their antennules, from six segments in juveniles to 11 in adults, increasing the total number of aesthetascs from 87 to 172. These differences from the expected slopes indicate that both antennules and the aesthetasc arrays scale much more slowly, giving small juveniles much larger antennules and aesthetascs relative to carapace width than large adults.

Variables affecting the gap width between aesthetascs are array width, aesthetasc diameter and length, and cuticle thickness. Aesthetasc diameter affects gap-width-to-diameter ratio and Reynolds number, the two major factors in the velocity of fluid flow through a aesthetasc array. Aesthetasc diameter scales with carapace width more slowly than all other measurements, changing by a factor of less than 1.5, while carapace width increases by a factor of seven. Aesthetasc length and cuticle thickness also affect the deflection of the aesthetascs. The aesthetasc lengths of small animals are considerably longer relative to their carapace width and their aesthetascs are disproportionately thick, suggesting that deflection of the aesthetasc during the downstroke, and therefore the splay ratio, remain similar over all carapace widths.

Flicking kinematics

Table 2 contains a summary of kinematic values (downstroke and return velocities and durations). Figure 4 shows kinematic values plotted as a function of carapace width. Across the size range, average downstroke velocities range from 3.8 to 14.5 cm s^{-1}, and average return-stroke velocities range from 1.38 to 7.82 cm s^{-1}. Duration of the downstroke and return stroke range from 8.0 to 14 ms and 16 to 43 ms, respectively. Downstroke and return stroke durations have no relationship with carapace width, staying a constant value throughout ontogeny. Reynolds numbers of downstroke and return strokes were calculated using aesthetasc diameters and mean downstroke and return velocities (Table 2) and plotted against carapace width in Figure 4. *Re* range from 0.27 to 1.17 during the downstroke, and return stroke *Re*'s ranged between 0.12 and 0.65. All *Re*'s remain in the sensitive range of $0.1 \leq Re \leq 10$. There are significant positive relationships between *Re* and carapace width for both the downstroke ($n = 13, p = 10^{-4}$) and return stroke ($n = 13, p = 7x10^{-3}$).

Aesthetasc Splay

The measured splay ratios of the downstroke, representing gap width, are reported in Table 2 and plotted against carapace width in Figure 4. Side and front splay ratios range from 1.56 to 2.99 and 2.00 to 4.35 across the carapace width range, respectively. However, both splay ratios have a small, negative slope when plotted against carapace width, indicating that splay ratios are relatively larger for smaller animals. These slopes are both significantly different from a slope of zero (see Table 2 for statistics). For small juveniles, increased splay ratios coupled with fewer aesthetascs per unit array width would increase the gap-width-to-diameter ratio, which would increase array leakiness for the range of Re seen during the downstroke.

Variable	n	Slope $\pm s_e$	r^2	y-intercept	p-value	95% confidence
Velocities ...						
Downstroke	13	0.51 ± 0.09	0.75	-0.08 ± 0.41	0.0001+	0.24 - 0.78
Return stroke	13	0.70 ± 0.1	0.83	-0.03 ± 0.44	0.007+	0.41 - 0.99
Duration ...						
Downstroke	13	(1.7 ± 0.7) x10^{-3}	0.33	0.02 ± 0.003	0.04*	(-0.30 - 3.7) x10^{-3}
Returnstroke	13	(1.3 ± 3)x10^{-3}	0.02	0.03 ± 0.01	< 0.0000001	(-6.7 - 8.3) x10^{-3}
Mean *Re*...						
Downstroke	9	0.46 ± 0.08	0.82	0.42 ± 0.21	0.0009 +	0.21 - 0.71
Return stroke	9	0.30 ± 0.03	0.93	0.38 ± 0.08	0.000003 +	0.21 - 0.40
Splay Ratios ...						
Front	9	-0.77 ± 0.37	0.37	-0.26 ± 1.67	0.04 *	-1.54 - 0
Side	8	-0.59 ± 0.19	0.62	-0.70 ± 0.84	0.01 *	-1.18 - 0.59

Table 2. Summary of sample size (n), regression slopes ($\pm$ standard error, s_e), correlation coefficients (r^2), y-intercepts, 95% confidence intervals for slope and significance for seven measured features. P-values for *slope = 0 and + slope=1.

Equations 2 and 3 provide a way to: (1) model the splay ratios based on measured morphometrics and an assumed, constant Young's modulus, E, to compare them with measured values; and (2) estimate the values of E during ontogeny based on measured splay ratios and morphometrics.

For part one, in equation 2 requires a hydrodynamic drag force on the aesthetascs. This force can be estimated by an equation for drag on a cylinder using the measured downstroke velocities, aesthetasc lengths and diameters, and cuticle thickness. I assumed that the hydrodynamic force, F, was distributed along the length of the aesthetasc and equal to,

$$F = \frac{1}{2} C_D \rho d L U^2 \tag{5}$$

where C_D is the experimentally determined drag coefficient on a cylinder at intermediate *Re* (Eq. 1) from Finn (1953). The calculated deflection was based on equations 2, 3, and 5. Mean downstroke velocity was used for U, and the density of seawater at 30‰, 15 °C (1025 kg m^{-3}) was used for ρ (Vogel, 1994). Each calculated deflection was then added to its corresponding array width measured from micrographs and divided by array width to find the modeled splay ratio. Young's modulus of cuticle was chosen as $E = 137$ MPa from Taylor et al. (2007) representing the cuticle of a one-hour post-molt blue crab.

Modeled splay ratios for part 1 are compared to splay ratios measured from kinematics in Figure 4. Although measured splay ratios tend to decrease with increasing carapace width, the modeled splay ratios estimated from morphometrics increase with size. This dramatic difference between the slopes is significant ($n = 14, p < 10^{-5}$) and shows that the structure of the aesthetascs alone does not account for the observed relationship between measured splay ratio and carapace width. For part two, the measured splay ratios and morphometric data were used to estimate real values of Young's modulus E using equation 2. Figure 4 shows results of the Young's modulus estimation. Calculated E range from 9.25 to 97.3 MPa, showing an increase in E during growth by an order of magnitude. The slope of the regression representing change in E during ontogeny is significantly different from zero ($n = 17, p = 0.03$), the expected slope if no change in E occurred.

DISCUSSION

Scaling relationships of array morphology and kinematics

Crustaceans, including brachyuran crabs, intermittently and discretely sample odors (sniff) by altering the kinematics of antennule flicking to increase fluid flow within their aesthetasc arrays during the downstroke and limit fluid flow within their arrays during the return stroke. Intermittent odor sampling occurs in this way only when antennule morphology and flicking kinematics are restricted to a certain range of Reynolds numbers (equation 1) in which small changes in antennule velocity, aesthetasc diameter, or gap widths between aesthetascs, which lead to dramatic effects on the fluid flow in an aesthetasc array (Koehl, 2006). In order for juvenile Oregon shore crabs to fall within this range, the antennules of juvenile crabs would need to operate in the transitional Re range despite their considerably smaller body size.

The allometric scaling of morphological and kinematic features of *Hemigrapsus oregonensis* antennules support this prediction. Aesthetasc diameter and length and array width number all increase much more slowly than predicted by isometry. These structures' slower rates of growth during ontogeny also slows the change in *Re* of the aesthetasc array and will potentially increase array leakiness compared to isometric arrays. In combination with flicking kinematics, the *Re* of the smallest juveniles were $Re > 0.10$. Despite the antennules of juvenile crabs operating at much lower *Re* than adults, they stay within the sensitive range in which dramatic shifts in fluid flow could still occur.

Scaling of aesthetasc deflection

Measured from kinematic data, the relationship between aesthetasc splay during the downstroke and carapace width supports the hypothesis that small juveniles have relatively larger splay ratios as compared to adult animals. Along with fewer total aesthetascs, larger splay ratios increase the gap width between aesthetascs in juvenile arrays during the downstroke. Since the *Re* of a small juvenile downstroke reaches only 0.27, not as high as the 1.2 seen as adults, this additional increase in gap width to diameter ratio could increase the leakiness within the array that was lost by lower velocities during the downstroke and smaller size of the aesthetascs.

Using the morphometric and kinematic measurements of one of the smallest juvenile crabs studied (carapace width = 4.9 mm, aesthetasc diameter = 5.69 μm, array width = 50 μm, number of aesthetascs in row = 6, front splay ratio = 4.34), more precise predictions can be made regarding leakiness through the array during flicking using the model provided in Cheer and Koehl (1987b). For a small crab, the calculated gap-width to aesthetasc-diameter for one row of aesthetascs is about 30, which combined with the $Re = 0.27$ during the downstroke, falls within the high leakiness range ($0.6 - 0.8$) (Cheer and Koehl, 1987b; Koehl, 2006). During the return stroke, gap-width to aesthetasc-diameter falls by two orders of magnitude to about 0.2, predicting very low leakiness (less than 0.2). These calculations suggest that the smallest crabs studied also have the necessary fluid dynamics to sniff. However, since the aesthetasc array is a more complicated three-dimensional structure than the single line of hairs used in the Cheer and Koehl model, measurements of fluid flow within the array and estimates of odor molecule capture are necessary to confirm these predictions.

The model of aesthetasc deflection as a bending beam based on morphometric data and constant material properties showed the opposite trend with increasing carapace width as the measured splay-ratio values (Figure 4). According to this model, splay ratios of small animals should be much smaller than adult animals and increase in value during growth. These results suggest that changes in the structural properties of the aesthetasc morphology (through the second moment of area *I* in equations 2 and **??**) do not sufficiently explain the relationship between splay ratio and carapace width.

When the beam-bending model is used in conjunction with the splay ratios measured through kinematics, it reveals a significant size-dependent relationship for the Young's modulus *E* of aesthetasc cuticle (Figure 4). These results indicate that the material properties of juvenile crab aesthetascs are different than those of the adults. Young's modulus of chitin has been show to vary during the ontogeny of insects based on the functional use of the tissue as well as during ecdysis for brachyurans, making such changes for juvenile crabs possible (Vincent and Wegst, 2004; Taylor et al., 2007). Having lower values of *E* as a juvenile would allow aesthetascs to deflect further with the same amount of applied force, producing greater splay ratios and a leakier array to capture odors during the downstroke.

Comparison to other crustacean species

Studies discrete odor sampling through a size range of the spiny lobster (*Panulirus argus*) and stomatopod (*Gonodactylus mutatus*) have shown that the antennule morphology and kinematics tend to maintain flicking aesthetasc *Re* within the transitional range where array leakiness is sensitive to small changes in velocity and gap width (Mead et al., 1999; Mead and Koehl, 2000; Goldman and Koehl, 2001). In these studies, the aesthetasc *Re* of *P. argus* was maintained over large changes in body size, whereas they increased in *G. mutatus* over growth. For shore crabs, aesthetasc *Re* increase but stay within the *Re* range in which small changes in velocity and gap width cause large changes in array leakiness.

Despite the significant differences between antennule and aesthetasc morphology, *H. oregonensis* individuals over a much larger body size range than previously studied show similar decrease in gap width between aesthetascs with increasing size. This effect seems to be accomplish by decreased values of *E* of aesthetasc cuticle in small juveniles animals leading to relatively larger splay ratios; an effect not observed in other species of crustaceans.

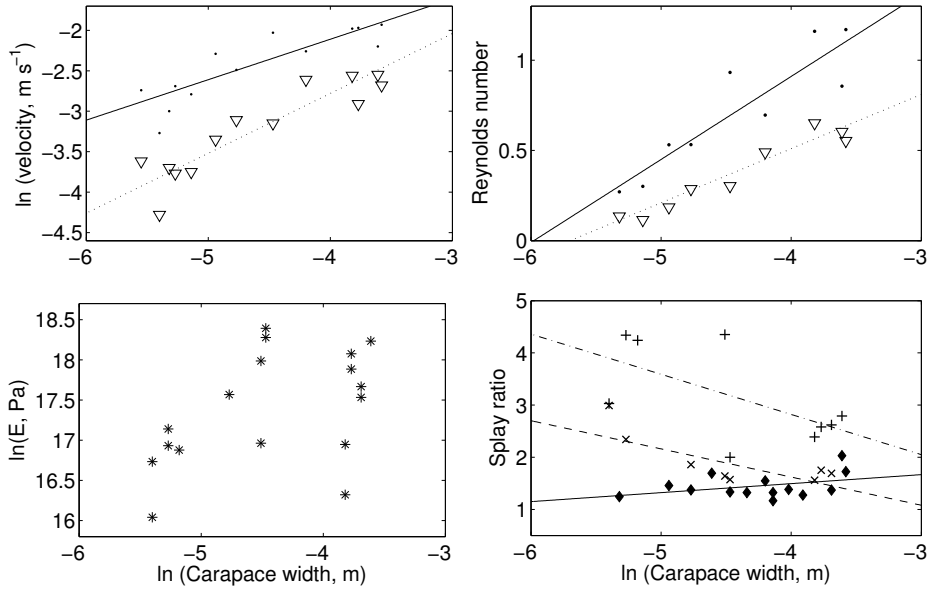

Figure 4. Select kinematic features plotted against natural-log carapace width. Top left: downstroke (dots) and return (triangles) velocities; top right: downstroke (dots) and return (triangles) Reynolds numbers; bottom left: estimated Young's modulus, E; bottom right: measured (front = +, side = x) and modeled (diamonds) splay ratios.

Odor capture in environmental flows

Most environments in which crabs are found are characterized by the existence of steady or transient ambient currents which could interfere with a crab's ability to capture odors discretely. Both *H. oregonensis* and the hermit crab, *Pagurus alaskensis*, preferentially orients its antennules during flicking in ambient currents so that the aesthetasc array is directly upstream to any flow present in its surroundings (Snow, 1973) (personal observation). Preferentially orienting the antennule in this way results in the ambient currents adding to the speed of the downstroke, making the water speed relative to the antennule much higher than flicking in still water. This increase in speed (U) would also increase drag on the hairs (F) according to equation 5 and the *Re* of the downstroke according to equation 1, splaying the hairs further apart than in still water conditions and increasing gap-to-diameter ratio of the array. Theoretically, ambient flow would increase the amount of new fluid delivered around the aesthetascs during the downstroke. During the return stroke, the antennule's direction reverses and the ambient flow instead subtracts some of the speed of the return stroke with respect to the antennule. Slower velocities result in lower *Re* for the aesthetascs (equation 1), and theoretically less fluid exchange within the array. Environmental flows would likely enhance odor sampling on the downstroke and limit escape of the sample during the return stroke.

ACKNOWLEDGEMENTS

I thank: M. Koehl for equipment, guidance, support, and critical reading of the manuscript; V. Rapp and P. Gursel for comments on manuscript; K. Dorgan for help in the field; G. Min and the UC Berkeley Electron Microscopy Lab; and the UC Berkeley Biomechanics group.

FUNDING

This work was supported by the Virginia and Robert Gill Chair and a MacArthur Foundation Fellowship (to M. Koehl); a Sigma-Xi Grant-in-Aid of Research to the author; and by a Traineeship to the author (National Science Foundation Integrative Graduate Education and Research Traineeship [#DGE-0903711] to R. Full, M. Koehl, R. Dudley, and R. Fearing).

REFERENCES

Abramoff, M., Magalhaes, P., and Ram, S. (2004). Image processing with ImageJ. *Biophotonics International*, 11(7):36–42.

Atema, J. (1995). Chemical signals in the marine-environment - dispersal, detection, and temporal signal analysis. *Proceedings of the National Academy of Science USA*, 92(1):62–66.

Atema, J. and Steinbach, M. (2007). *Evolutionary ecology of social and sexual systems: crustaceans as model organisms.*, chapter Chemical communication and social behavior of the lobster *Homarus americanus* and other decapod crustacea, pages 115–144. Oxford Univ. Press, NY.

Caldwell, R. (1979). Cavity occupation and defensive behavior in the stomatopod *Gonodactylus festai* - evidence for chemically mediated individual recognition. *Animal Behavior*, 27:194–201.

Cheer, A. and Koehl, M. (1987a). Fluid-flow through filtering appendages of insects. *IMA J Math Appl Med Biol*, 4(3):185–199.

Cheer, A. and Koehl, M. (1987b). Paddles and rakes - fluid-flow through bristled appendages of small organisms. *Journal of Theoretical Biology*, 129(1):17–39.

Derby, C. and Atema, J. (1988). *Sensory Biology of Aquatic Animals*, chapter Chemoreceptor cells in aquatic invertebrates: peripheral mechanisms of chemical signal processing in decapod crustaceans., pages 365–385. Springer-Verlag, New York.

Devore, J. (1987). *Probability and statistics for engineering and the sciences*. Brooks/Cole, Monterey, CA.

Diaz, H., Orihuela, B., Forward, R., and Rittschof, D. (1999). Orientation of blue crab, *Callinectes sapidus* (Rathbun), megalopae: Responses to visual and chemical cues. *Journal of Experimental Marine Biology and Ecology*, 233(1):25–40.

Dodds, P., Rothman, D., and Weitz, J. (2001). Re-examination of the "3/4-law" of metabolism. *Journal of Theoretical Biology*, 209(1):9–27.

Dusenbery, D. (1992). *Sensory ecology: How organisms acquire and respond to information.* W.H. Freeman.

Ferner, M., Smee, D., and Chang, Y. (2005). Cannibalistic crabs respond to the scent of injured conspecifics: Danger or dinner? *Marine Ecology Progess Series*, 300:193–200.

Finn, R. (1953). Determination of the drag on a cylinder at low reynolds numbers. *Journal of Applied Physics*, 24(6):771–773.

Gherardi, F. and Tricarico, E. (2007). Can hermit crabs recognize social partners by odors? and why? *Marine and Freshwater Behavioral Physiology*, 40(3):201–212.

Gherardi, F., Tricarico, E., and Atema, J. (2005). Unraveling the nature of individual recognition by odor in hermit crabs. *Journal of Chemical Ecology*, 31(12):2877–2796.

Gleeson, R. (1980). Pheromone communication in the reproductive behavior of the blue crab, *Callinectes sapidus*. *Marine Behavior and Physiology*, 7(2):119–134.

Gleeson, R. (1982). Morphological and behavioral identification of the sensory structures mediating pheromone reception in the blue crab, *Callinectes sapidus*. *Biological Bulletin*, 163(1):162–171.

Gleeson, R., Hammar, K., and Smith, P. (2000a). Sustaining olfaction at low salinities: Mapping ion flux associated with the olfactory sensilla of the blue crab *Callinectes sapidus*. *Journal of Experimental Biology*, 203(20):3145–3152.

Gleeson, R., McDowell, L., Aldrich, H., Hammar, K., and Smith, P. (2000b). Structure of the aesthetasc (olfactory) sensilla of the blue crab, callinectes sapidus: Transformations as a function of salinity. *Cell Tissue Res*, 301(3):423–431.

Goldman, J. and Koehl, M. (2001). Fluid dynamic design of lobster olfactory organs: High speed kinematic analysis of antennule flicking by *Panulirus argus*. *Chemical Senses*, 26(4):385–398.

Goldman, J. and Patek, S. (2002). Two sniffing strategies in palinurid lobsters. *Journal of Experimental Biology*, 205(24):3891–3902.

Hallberg, E., Johansson, K., and Wallen, R. (1997). Olfactory sensilla in crustaceans: Morphology, sexual dimorphism, and distribution patterns. *Int. J. Insect Morphol. Embryol.*, 26(3-4):173–180.

Hallberg, E. and Skog, M. (2011). *Chemical communication in Crustaceans*, chapter Chemosensory sensilla in crustaceans, pages 103–121. Springer, New York.

Hart, J. (1935). The larval development of British Columbia brachyura. i. Xanthidae, Pinnotheridae (in part) and Grapsidae. *Canadian J. Res.*, 12(4):411–432.

Hazlett, B. (1969). Individual recognition and agonistic behaviour in *Pagurus bernhardus*. *Nature*,

222(5190):268–269.
Keller, T., Powell, I., and Weissburg, M. (2003). Role of olfactory appendages in chemically mediated orientation of blue crabs. *Marine Ecology Progess Series*, 261:217–31.
Kepecs, A., Uchida, N., and Mainen, Z. (2006). The sniff as a unit of olfactory processing. *Chemical Senses*, 31(2):167–179.
Koehl, M. (2006). The fluid mechanics of arthropod sniffing in turbulent odor plumes. *Chemical Senses*, 31(2):93–105.
Lecchini, D., Mills, S., Brie, C., Maurin, R., and Banaigs, B. (2010). Ecological determinants and sensory mechanisms in habitat selection of crustacean postlarvae. *Behavioral Ecology*, 21(3):599–607.
Lincoln, R. and Sheals, J. (1979). *Invertebrate animals collection and preservation*. Cambridge Univ. Press, Cambridge.
Loudon, C., Best, B., and Koehl, M. (1994). When does motion relative to neighboring surfaces alter the flow-through arrays of hairs. *Journal of Experimental Biology*, 193:233–254.
Mead, K. and Koehl, M. (2000). Stomatopod antennule design: The asymmetry, sampling efficiency and ontogeny of olfactory flicking. *Journal of Experimental Biology*, 203(24):3795–3808.
Mead, K., Koehl, M., and O'Donnell, M. (1999). Stomatopod sniffing: The scaling of chemosensory sensillae and flicking behavior with body size. *Journal of Experimental Marine Biology and Ecology*, 241(2):235–261.
Moore, P., Atema, J., and Gerhardt, G. (1991). Fluid dynamics and microscale chemical movement in the chemosensory appendages of the lobster, *Homarus americanus*. *Chemical Senses*, 16(6):663–674.
Pardieck, R., Orth, R., Diaz, R., and Lipcius, R. (1999). Ontogenetic changes in habitat use by postlarvae and young juveniles of the blue crab. *Marine Ecology Progess Series*, 186:277–238.
Schmidt, B. and Ache, B. (1979). Olfaction: responses of a decapod crustacean are enhanced by flicking. *Science*, 205:204–206.
Schoenfeld, T. (2006). Special issue: What's in a sniff?: The contributions of odorant sampling to olfaction. *Chemical Senses*, 31(2):91–92.
Schuech, R., Stacey, M., Barad, M., and Koehl, M. (2012). Numerical simulations of odorant detection by biologically inspired sensor arrays. *Bioinspiration and Biomimetics*, 7(1):016001.
Shabani, S., Kamio, M., and Derby, C. (2009). Spiny lobsters use urine-borne olfactory signaling and physical aggressive behaviors to influence social status of conspecifics. *Journal of Experimental Biology*, 212(15):2464–2474.
Skog, M. (2009). Male but not female olfaction is crucial for intermolt mating in European lobsters (*Homarus gammarus* L.). *Chemical Senses*, 34(2):159–169.
Snow, P. (1973). Antennular activities of hermit crab, *Pagurus alaskensis* (Benedict). *Journal of Experimental Biology*, 58(3):745–765.
Stacey, M., Mead, K., and Koehl, M. (2002). Molecule capture by olfactory antennules: Mantis shrimp. *Journal of Mathematical Biology*, 44(1):1–30.
Taylor, J., Hebrank, K., and Kier, W. (2007). Mechanical properties of the rigid and hydrostatic skeletons of molting blue crabs, *Callinectes sapidus* Rathbun. *Journal of Experimental Biology*, 210(24):4272–4278.
Vincent, J. and Wegst, U. (2004). Design and mechanical properties of insect cuticle. *Arthropod Structure and Development*, 33(3):187–199.
Vogel, S. (1994). *Life in Moving Fluids: The Physical Biology of Flow*. Princeton University Press, Princeton, NJ.
Vogel, S. (2003). *Comparative Biomechanics: Life's Physical World*. Princeton University Press, Princeton, NJ.
Wachowiak, M. (2011). All in a sniff: olfaction as a model for active sensing. *Neuron*, 71:962–973.
Wainwright, S., Biggs, W., Currey, J., and Gosline, J. (1982). *Mechanical Design in Organisms*. Princeton University Press, Princeton, NJ.
Zimmer, R. and Butman, C. (2000). Chemical signaling processes in the marine environment. *Biological Bulletin*, 198(2):168–187.